Highlights

Evolution of the disk of π Aqr: from near-disappearance to a strong maximum

Yaël Nazé, Gregor Rauw, Joan Guarro Fló, Arnold De Bruin, Olivier Garde, Olivier Thizy, Franck Houpert, Ernst Pollmann, Carl J. Sawicki, Marco Leonardi, Malin Moll, Christoph T. Quandt, Paolo Berardi, Tim Lester, Patrick Fosanelli, André Favaro, Jean-Noël Terry, Keith Graham, Benjamin Mauclaire, Terrence Bohlsen, Michel Pujol, Etienne Bertrand, Erik Bryssinck, Valérie Desnoux, Patrick Lailly, Jacques Montier, Massimiliano Mannucci, Nico Montigiani, Albert Stiewing, James Daglen, Christian Kreider, Thierry Lemoult, Tony Rodda

- The disk surrounding the primary component of π Aqr nearly disappeared in early 2014.

- The disk has slowly recovered, now reaching strengths not seen in three decades.

- This evolution in line strength is accompanied by changes in disk structure.

Evolution of the disk of π Aqr: from near-disappearance to a strong maximum

Yaël Nazé[a,*], Gregor Rauw[a], Joan Guarro Fló[b], Arnold De Bruin[c], Olivier Garde[d], Olivier Thizy[e], Franck Houpert[f], Ernst Pollmann[g], Carl J. Sawicki[h], Marco Leonardi[i], Malin Moll[j], Christoph T. Quandt[k], Paolo Berardi[l], Tim Lester[m], Patrick Fosanelli[n], André Favaro[o], Jean-Noël Terry[p], Keith Graham[q], Benjamin Mauclaire[r], Terrence Bohlsen[s], Michel Pujol[t], Etienne Bertrand[u], Erik Bryssinck[v], Valérie Desnoux[w], Patrick Lailly[x], Jacques Montier[y], Massimiliano Mannucci[z], Nico Montigiani[z], Albert Stiewing[aa], James Daglen[ab], Christian Kreider[ac], Thierry Lemoult[ad], Tony Rodda[ae]

[a]*Groupe d'Astrophysique des Hautes Energies, STAR, Université de Liège, Quartier Agora (B5c, Institut d'Astrophysique et de Géophysique), Allée du 6 Août 19c, B-4000 Sart Tilman, Liège, Belgium*
[b]*Balmes 2, 08784 Piera (Barcelona), Spain*
[c]*Gooiergracht 91, 1250–1252 Laren, Netherlands*
[d]*Observatoire de la Tourbière, 38690 Chabons, France*
[e]*Observatoire de la Belle Étoile, 38420 Revel, France*
[f]*Verny Observatory, 57420 Verny, France*
[g]*Emil-Nolde-Strasse 12, 51375 Leverkusen, Germany*
[h]*PO box 141, Alpine, Texas 79831, USA*
[i]*Cotoletta Observatory, Via Matteotti 81, 20064 Gorgonzola (MI), Italy*
[j]*Kapellenkamp 21, 23569 Lübeck, Germany*
[k]*Uhlandstrasse 11d, 23617 Stockelsdorf, Germany*
[l]*Bellavista Observatory, Via Carlo De Paulis, 15 - 67100 L'Aquila, Italy*
[m]*1178 Mill Ridge Road, Arnprior, ON, K7S3G8, Canada*
[n]*39 Rue des Songes , 68850 Staffelfelden, France*
[o]*19 Bd Carnot, 21000 Dijon, France*
[p]*Observatoire du Pilat, 42660 Tarentaise, France*
[q]*23746 Schoolhouse Road, Manhattan, Illinois, USA*
[r]*Observatoire du Val de l'Arc, 13530 Trets, France*
[s]*Mirranook Observatory, Armidale NSW, Australia*
[t]*Rue des Pins, 31700 Beauzelle, France*
[u]*105 Bd de la Côte de Beauté, 17640 Vaux Sur Mer, France*
[v]*Eyckensbeekstraat 2, 9150 Kruibeke, Belgium*
[w]*13 Rue Saint Charles, 75015 Paris, France*
[x]*Observatoire Canigou, 64000 Pau, France*
[y]*Centre d'Astronomie de La Couyère, 35320 La Couyère, France*
[z]*Osservatorio Astronomico Margherita Hack, Lasra a Signa (FI), Italy*
[aa]*16210 N Desert Holly Dr, Sun City, AZ 85351, USA*
[ab]*33 Joy Rd, PO Box 196, Mayhill, New Mexico 88339, USA*
[ac]*17 Rue Schelbaum, 68360 Soultz, France*
[ad]*Chelles Observatory, 23 Avenue Henin, 77500 Chelles, France*
[ae]*1 Rivermede, Ponteland, Newcastle upon Tyne NE20 9XA, UK*

Abstract

Some Be stars display important variability of the strength of the emission lines formed in their disk. This is notably the case of π Aqr. We present here the recent evolution of the Be disk in this system thanks to spectra collected by amateur spectroscopists since the end of 2013. A large transition occurred: the emission linked to the Be disk nearly disappeared in January 2014, but the disk has recovered, with a line strength now reaching levels only seen during the active phase of 1950–1990. In parallel to this change in strength occurs a change of disk structure, notably involving the disappearance of the strong asymmetry responsible for the V/R modulation.

Keywords: stars: Be, stars: individual (π Aqr)

1. Introduction

π Aqr (HD212571) is a nearby (d=257–331 pc, Bailer-Jones et al. 2018) binary system comprising a Be primary (Bjorkman et al., 2002). Because of its brightness (V=4.64), it has been studied for a long time, both in photometry and spectroscopy. However, it was only recently found to belong to the peculiar class of γ-Cas stars, which gathers Be stars with unusually bright and hard X-ray emission (Nazé et al., 2017, see also Smith et al. 2016 for a detailed review on such objects).

Variability is commonly seen in Be stars in general and

---

*Corresponding author, FNRS research associate
Email address: ynaze@uliege.be (Yaël Nazé)

in π Aqr in particular. After an active phase in 1950–1990, π Aqr went through a very weak emission phase in 1996–2000. Bjorkman et al. (2002) extensively studied it, which allowed them to detect the individual signatures of the two components of the system. As the disk had (nearly) disappeared, the Hα line appeared mostly in absorption. This absorption component belonged to the massive primary. Superimposed on it were weak emissions due to the tenuous remnants of the disk and another weak emission displaying opposite motion with respect to the absorption. This emission was therefore attributed to the secondary star of the system. Bjorkman et al. (2002) measured the radial velocities (RVs) of the absorption and the secondary emission, and used them to derive the system's properties. π Aqr has an orbital period of 84.1 d and a mass ratio of 0.16 which suggests a 2–3 $M_\odot$ secondary star to the B1 primary.

Zharikov et al. (2013) further examined the variations of the Hα line between 2004 and 2013. At that time, the activity oscillated between low and moderate states, without reaching the high levels of the active phase. Using tomographic techniques, Zharikov et al. (2013) showed that the disk was influenced by the presence of the companion, with the brightest regions located on the outer part of the disk facing the secondary.

As the star continues to evolve, we examine in this contribution the behaviour of π Aqr over the last six years. The observations used to this aim and their treatment are presented in the next section, while results are presented in detail in Sect. 3, with a summary ending the paper.

2. Observations and data reduction

Because of their brightness and varying character, Be stars are regularly observed by the amateur astronomer community. Such observations may be photometric or spectroscopic, in which case they usually cover the Hα line. The Be Star Spectra (BeSS) open-access database[1] (Neiner et al., 2011) collects and centralizes the spectra of Be stars taken by amateurs and professionals to ensure their legacy to the astronomical community as a whole. We have downloaded from it all spectra of π Aqr taken between Oct. 2013 and Jan. 2019 (i.e. since the analysis of Zharikov et al. 2013). All these spectra have been taken by amateurs, co-authors of this paper, who reduced the data in a standard way. More information on these data can be found on the BeSS website.

In addition to BeSS data, two German amateurs (C.T. Quandt and M. Moll) provided additional spectra of π Aqr in 2017–2018. They were taken using a 5 inch Schmidt-Cassegrain telescope equipped with a LHiRes III spectrograph. The detector was a Sony IMX 674 CCD in 2017 and a Sony IMX 694 CCD in 2018. Several exposures were taken and combined to get the final 13 spectra. Data reduction was carried out in ESO-MIDAS in a standard way. For wavelength calibration of the spectra, the internal NeAr lamp of the spectrograph was used but recalibration, performed using telluric lines, enabled them
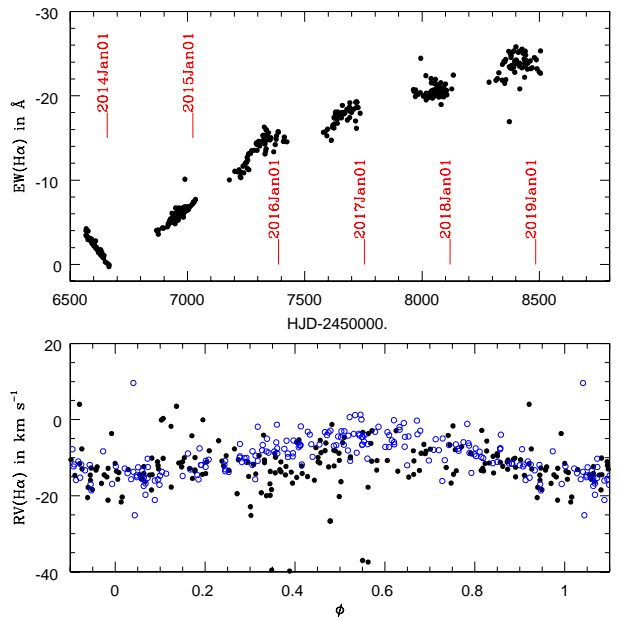
Figure 1: *Top:* Evolution of Hα *EWs* in π Aqr since October 2013. *Bottom:* Measured *RVs* (Oct. 2013–Feb. 2016 shown in black dots and July 2016–Jan. 2019 in blue circles), phased with average ephemeris from Bjorkman et al. (2002, i.e. P=84.1 d and HJD_0=2 450 275.5).

to improve the wavelength accuracy (on average, the precision is 3 km s^{-1}).

In total, our dataset consists of 379 Hα spectra of π Aqr. The annual visibility season typically extends from June to January of the following year, but two-thirds of spectra were actually taken in October–December. Because we gather the contributions of different observers from various places, the spectra were taken in various meteorological and instrumental conditions. In particular, the used telescopes had diameters between 5 and 20 inches, spectrographs had resolving powers between 5000 and 20 000 (with the exception of two low-resolution spectra taken at R = 600 on 2015-11-08 by C. Kreider and 2018-08-22 by T. Rodda). Exposure times ranged from 200s to 7800s and the vast majority of spectra are of good quality (SNR of at least 100 in 87% of spectra).

While the amateurs' spectra were roughly normalized, we have further processed them, first by correcting for telluric absorptions within IRAF using the template of Hinkle et al. (2000) then by applying a final normalization using continuum windows and a low-order polynomial. The continuum windows were adapted to the spectral range: in some cases, the range covered by the spectra was rather small hence the continuum windows had to be taken close to the line and the normalization was then poorer when the line was stronger and broader, which was the case in recent years (this explains some additional scatter of measurements for the last observing year).

3. Results

After applying the individual heliocentric corrections[2], we measured the moments of the Hα line in all normalized spectra over the velocity interval $-540\,\mathrm{km\,s^{-1}}$ to $540\,\mathrm{km\,s^{-1}}$ (using a rest wavelength of 6562.85 Å). No correction for the underlying photospheric absorption was performed, as in Zharikov et al. (2013) but contrary to Bjorkman et al. (2002). The resulting moments are listed in the fifth to seventh columns of Table 1. The zeroth-order moment ($M_0 = \sum(F_i - 1)$) corresponds to the equivalent width (EW), i.e. it provides the width of a rectangular line of unity amplitude with the same integrated area as the observed line. Note that, in this paper, emission lines have negative EWs while absorptions have positive EWs. The first-order moment ($M_1 = \sum(F_i - 1) \times v_i / \sum(F_i - 1)$) provides a flux-weighted centroid for the line, i.e. its RV. The second-order moment ($M_2 = \sum(F_i - 1) \times (v_i - M_1)^2 / \sum(F_i - 1)$) provides the square of the line width; it would be equal to σ^2 if the line were a centered Gaussian. In parallel, we have also measured the height above continuum of the blue and red peaks and Table 1 provides their ratio (traditionally called V/R). Comparing our results with Zharikov et al. (2013), who did not use moments to derive EWs, we found that their EWs and V/R values for the data in October 2013 agree well with ours. We also compared the results for different observers (those who provided at least 20 spectra) and found no systematic difference between them. As in Zharikov et al. (2013), we do not provide formal errors (e.g. from error propagation) on our measurements as the scatter of values are best representative of the actual errors, due to noise but also to normalization errors, imperfect telluric corrections, wavelength calibration errors,... We now examine each diagnostic in turn.

3.1. EWs

Figure 1 shows the evolution of the EW over recent years. As can be seen, it decreases at the end of 2013 and then reaches ~ 0 Å in January 2014. At that time, the emission had not completely disappeared, however. Rather, the emission component was so weak that the absorption component was revealed. Its strength nearly compensated that of the emission, leading to a ~ 0 Å EW value for the overall line. The line did not reach the absorption-dominated stage seen by Bjorkman et al. (2002), but it was without doubt in a very low emission state. Such (nearly) disappearance of the emission is not infrequent in π Aqr. For example, McLaughlin (1962) reported an absence of bright emission lines in 1936-7, 1944-5, and 1950 while Zharikov et al. (2013) reported another low emission state ($|EW| < 1$ Å) from mid-2006 to mid-2007.

After that minimum, the emission monotonically increased over the years, reaching EW values around -25 Å in the last year. This represents a large change compared to recent years. Indeed, between 2004 and 2013, the Hα line displayed at most a moderate emission, with absolute EW values varying between 1
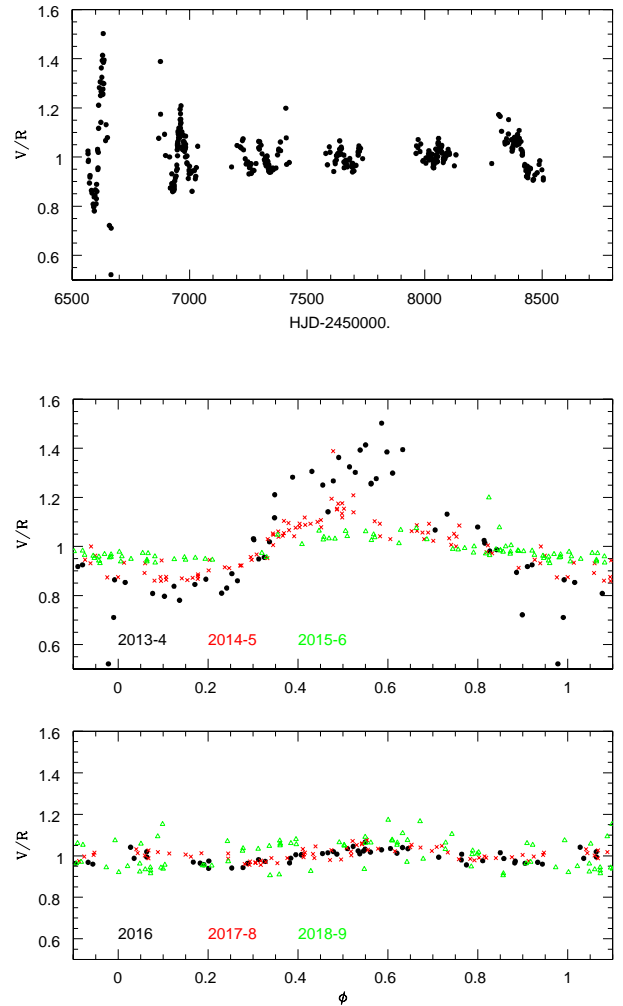
Figure 2: Evolution of V/R with time (top panel) or phase (middle and bottom panels), using the same ephemeris as for the RVs in Fig. 1). In the lower panels, different colors and symbols are used to identify the observing seasons: black dots for 2013-4, red crosses for 2014-5, and empty green triangles for 2015-6 in the middle panel; black dots for 2016, red crosses for 2017-8, and empty green triangles for 2018-9 in the bottom panel.

---

[2]Note that the keyword BSS_RQVH in the BeSS header provides the opposite of that correction.

and 11 Å (Zharikov et al., 2013). Starting in Fall 2015, the *EWs* exceeded such values, more than doubling in recent years. Figure 1 in Bjorkman et al. (2002) shows that large *EW* values (–20 to –40 Å, after correction for photospheric absorption) were previously observed between 1950 and 1990. π Aqr thus seems to have entered a new active phase, with the low activity state of previous years coming to an end.

3.2. RV

Since π Aqr is a binary, its lines should regularly shift with orbital phase. Figure 1 shows the velocities of the Hα line, phased with the ephemeris of Bjorkman et al. (2002). While the scatter is not negligible, a clear sinusoidal variation, independent of the observing season, is detected, as could be expected.

3.3. V/R

When in emission, the Hα line of π Aqr usually appears double-peaked. This is a common feature in Be stars seen under a high inclination. In a significant fraction of such stars, monitorings revealed variations of the amplitude of the violet peak with respect to that of the red one (see e.g. Porter & Rivinius, 2003). In π Aqr, their ratio, called *V/R*, was found to undergo a sinusoidal variation with the same periodicity as the orbital motions (Zharikov et al., 2013). This modulation was attributed to the disk asymmetry triggered by the presence of the companion (Zharikov et al., 2013).

Figure 2 shows the evolution of the *V/R* ratio with time and orbital phase. It clearly appears that the *V/R* modulation depends on the line strength: the largest amplitudes in *V/R* occur when the line is weakest. However, this is not a simple dilution effect: in the most recent data, the *V/R* modulation actually disappears, with *V/R* ratios simply scattered over phase.

3.4. Line profile

The top panel of Fig. 3 shows the evolution of the line profile variations with time. One profile per observing season is shown, except for 2013-4 for which the profiles at the beginning and end of the season are displayed. The double-peaked nature of the profile remained over the years. We have not yet reached a state with a single-peaked profile (Slettebak & Reynolds, 1978) but the situation appears close to the asymmetric profile with two barely distinguishable peaks reported by Andrillat & Fehrenbach (1982).

However, large changes in the profiles are detected besides the obvious variations in strength. First, the width of the line profile has continuously decreased as the line strength increased. This can be best seen in the bottom panel of Fig. 3, where the second-order moment[3] evolves from ~230 to ~210 km s^{-1} between Fall 2014 and Winter 2018-9. This is in line with McLaughlin (1962), who already noted that reappearing Hydrogen emissions are broader than usual, leading to

Figure 3: Evolution of the Hα line profile and its width (as measured by the second-order moment) since Oct. 2013. In the top panel, the individual spectra are shifted by a constant step of 0.3 to facilitate the comparison and velocities are heliocentric.

a width decrease afterwards. Second, at the same time, the two peaks clearly move closer to each other, with a separation changing from ~320 to ~140 km s^{-1}. If linked to Keplerian rotation of the disk, this suggests an increase in the radial extension of the disk (Hummel, & Vrancken, 1995). The observed separation decrease translates into an increase in the radius of the Hα emission region by a factor of ~5 (Zamanov et al., 2019, see their eq. 2).

The change in behaviour of the *V/R* ratios and in the line profile can be taken as indicating a change in the disk structure. To further examine this transition, we have performed a tomographic analysis of the profiles in each season. This technique assumes that the emitting gas is stationary in the rotating frame of the binary, i.e. that the line profile variations are only due to our changing viewing angle because of the orbital motion (Horne, 1991). In this case, each emitting parcel is associated to a specific (v_x, v_y) pair, where the x-axis points from the primary to the secondary and the y-axis has the same direction as the velocity vector of the secondary. The radial velocity of the emission, as seen by an observer on Earth, is then given at any phase by $v(\phi_t) = -v_x \cos(2\pi\phi_t) + v_y \sin(2\pi\phi_t) + v_z$ where ϕ_t is zero at the conjunction with the secondary star in front[4]. We used an implementation of Doppler tomography relying on a Fourier-filtered back-projection algorithm, as in Rauw et al. (2002, 2005).

To perform this analysis, we have separated the spectra by

---

[3]In 2013-4, the line profile is a mix of absorption and emission with similar strengths, hence the first and second-order moments are not fully representative of the actual centroid and width of the emission.
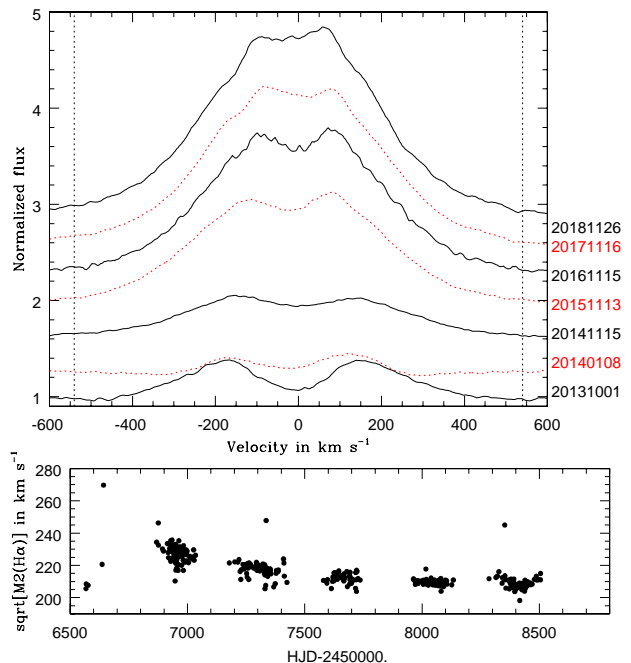
[4]Therefore $\phi_t = \phi + 0.25$, where the orbital phase ϕ used in the rest of the paper refers to the ephemeris of Bjorkman et al. (2002).

observing season, excluding the two taken at very low resolution ($R = 600$) and those with $EW > -0.5\,\text{Å}$ (i.e. with a line strongly affected by absorption). Since the Hα line strength significantly changes even during a single observing season, we have divided the individual line fluxes by the EWs. Furthermore, the spectra were weighted to achieve an orbital phase coverage as homogeneous as possible (i.e. if several spectra were taken at similar phases, each one had a reduced weight). Finally, the Doppler maps were calculated twice: first by considering all available spectra in each season and second by considering only a subset of spectra taken during that season by a single observer (e.g. J. Guarro-Fló in 2013-4, A. De Bruin in 2016). The latter case provides more homogeneity (a single observer, a single observing place, a single instrument), which enables us to check whether combining data from several sources caused problems. We found that the maps were similar, but with lower SNR with fewer spectra, hence Fig. 4 presents only the ones derived from all available spectra. We recall that they provide a measure of the line flux in the *velocity* space, which does not directly reflect *spatial* distribution. In particular, emission linked to a Keplerian disk should appear as an annulus with inner and outer regions inverted in velocity space - indeed, the inner disk regions have the largest velocities hence appear on the outer part of the Doppler map.

In the maps, the Be disk of π Aqr appears as a large structure of approximately annular form. The inner radius of this ring (central red contour in Fig. 4), the position of the maximum emission regions (blue and magenta contours in Fig. 4), as well as the (a)symmetric character of the overall structure appear to change with time. At first, the disk shows a strong asymmetry peaking on the secondary side, as found by Zharikov et al. (2013). However, this asymmetry subsequently decreases and nearly disappears after 2015 or 2016. This may seem to contradict the previous results of Zharikov et al. (2013) who had found that the overall inhomogeneity in disk surface brightness was larger when the line was stronger, but we recall that the regime in line strength probed in that paper is very different than observed since Fall 2015. There is thus no contradiction, only a change in behaviour in the most active phase. The strong reduction in disk asymmetry in Doppler maps is in line with the disappearance of the V/R modulation. At the same time, the maps indicate that the inner edge of the disk gets closer (in velocity) to the Be star, suggesting again a larger disk extension.

4. Conclusion

In this paper, we report on changes in the Hα line profile of the Be star π Aqr since the last published monitoring (Zharikov et al., 2013). During Winter 2013-2014, the emission of π Aqr became very weak but did not disappear completely. Its strength was then similar to that of the photospheric absorption. Since then, the emission has monotonically increased and is now reaching levels only seen during the last "active" phase, in 1950-1990. In this process, the Be disk of π Aqr appears to have extended and to have lost the strong asymmetry responsible for the V/R modulation of the line peaks.

References

Andrillat, Y., & Fehrenbach, C. 1982, A&AS, 48, 93

Bailer-Jones, C. A. L., Rybizki, J., Fouesneau, M., Mantelet, G., & Andrae, R. 2018, AJ, 156, 58

Bjorkman, K. S., Miroshnichenko, A. S., McDavid, D., & Pogrosheva, T. M. 2002, ApJ, 573, 812

Hinkle, K., Wallace, L., Valenti, J., & Harmer, D. 2000, Visible and Near Infrared Atlas of the Arcturus Spectrum 3727-9300 A ed. Kenneth Hinkle, Lloyd Wallace, Jeff Valenti, and Dianne Harmer. (San Francisco: ASP) ISBN: 1-58381-037-4, 2000.,

Horne K., in "Fundamental Properties of Cataclysmic Variable Stars: 12th North American Workshop on Cataclysmic Variables and Low Mass X-ray Binaries", Shafter A.W. (Ed.), SDSU Press (1991), p.23

Hummel, W., & Vrancken, M. 1995, A&A, 302, 751.

McLaughlin, D. B. 1962, ApJS, 7, 65

Nazé, Y., Rauw, G., & Cazorla, C. 2017, A&A, 602, L5

Neiner, C., de Batz, B., Cochard, F., et al. 2011, AJ, 142, 149

Porter, J. M., & Rivinius, T. 2003, PASP, 115, 1153

Rauw, G., Crowther, P. A., Eenens, P. R. J., Manfroid, J., & Vreux, J.-M. 2002, A&A, 392, 563

Rauw, G., Crowther, P. A., De Becker, M., et al. 2005, A&A, 432, 985

Slettebak, A., & Reynolds, R. C. 1978, ApJS, 38, 205

Smith, M. A., Lopes de Oliveira, R., & Motch, C. 2016, Advances in Space Research, 58, 782

Zamanov, R., Stoyanov, K. A., Wolter, U., Marchev, D., & Petrov, N. I. 2019, A&A, 622, A173

Zharikov, S. V., Miroshnichenko, A. S., Pollmann, E., et al. 2013, A&A, 560, A30

Table 1: Journal of the observations of π Aqr taken between Oct. 2013 and Jan. 2019, as well as the associated measurements of the Hα line. As observing log are provided the observing date, observer ID (using the BeSS nickname when applicable, initials otherwise), and instrument details (telescope size and resolving power of spectrograph). The provided Hα results are EWs (0th-order moment), RVs (1st-order moment), widths (squared root of the 2nd-order moment) and V/R ratios. Note that, when the line combines absorption and emission (i.e. 0th-order moment is close to zero), the higher order moments become less representative of the properties of the emission component. Low-resolution data (R=600) also have imprecise higher order moments.

Date (YYYYMMDD)	HJD $-2\,450\,000$	Observer	tel size/R (mm)/	EW (Å)	RV (km s^{-1})	width (km s^{-1})	V/R
20131001	6567.358	epollmann	400/20000	-3.99	-13.4	206	1.025
20131001	6567.476	jguarroflo	406/5000	-3.45	-2.8	188	1.013
20131002	6568.427	fhoupert	280/17000	-4.23	-5.6	208	0.981
20131004	6569.696	csawicki	356/15000	-3.38	-14.0	188	0.987
20131007	6573.425	jguarroflo	406/5000	-3.27	-10.4	181	0.894
20131009	6575.461	jguarroflo	406/5000	-2.95	-14.7	169	0.918
20131010	6576.336	epollmann	400/20000	-3.97	4.0	208	0.925
20131016	6582.332	jguarroflo	406/5000	-3.03	-3.7	175	0.864
20131018	6584.309	jguarroflo	406/5000	-3.10	-20.3	170	0.853
20131023	6589.455	jguarroflo	406/5000	-2.71	-14.6	145	0.808
20131026	6591.654	csawicki	356/15000	-2.99	-0.1	171	0.797
20131027	6593.453	jguarroflo	406/5000	-2.49	-1.8	131	0.837
20131028	6594.472	jguarroflo	406/5000	-2.65	3.5	155	0.780
20131031	6597.365	jguarroflo	406/5000	-2.52	-4.2	140	0.845
20131102	6599.414	jguarroflo	406/5000	-2.28	-0.1	114	0.866
20131105	6602.348	jguarroflo	406/5000	-2.21	-5.5	99	0.809
20131106	6603.305	jguarroflo	406/5000	-2.16	-12.2	100	0.830
20131107	6604.280	jguarroflo	406/5000	-2.29	-13.3	124	0.889
20131108	6605.319	jguarroflo	406/5000	-2.11	-7.7	91	0.860
20131111	6608.309	jguarroflo	406/5000	-2.01	-22.9	74	1.031
20131111	6608.406	bmauclaire	300/16000	-2.79	-25.2	125	1.027
20131112	6609.298	jguarroflo	406/5000	-1.92	-14.3	6	0.949
20131113	6610.332	jguarroflo	406/5000	-1.98	-19.2	78	0.955
20131114	6611.311	jguarroflo	406/5000	-2.01	-20.0	98	1.019
20131115	6612.261	jguarroflo	406/5000	-1.97	-18.4	75	1.117
20131115	6612.290	epollmann	400/20000	-1.97	-39.5	87	1.211
20131119	6615.636	csawicki	356/15000	-1.73	-39.8	84	1.282
20131122	6619.242	jguarroflo	406/5000	-1.69	-45.3	59	1.306
20131124	6621.280	jguarroflo	406/5000	-1.40	-11.4	137	1.250
20131125	6622.269	jguarroflo	406/5000	-1.71	-8.2	11	1.141
20131126	6623.251	jguarroflo	406/5000	-1.47	-26.6	118	1.267
20131127	6624.254	jguarroflo	406/5000	-1.47	-59.4	117	1.363
20131129	6626.283	jguarroflo	406/5000	-1.41	-40.8	122	1.324
20131130	6627.358	jguarroflo	406/5000	-1.46	-54.4	105	1.302
20131201	6628.270	jguarroflo	406/5000	-1.31	-42.0	137	1.393
20131202	6629.276	epollmann	400/20000	-1.75	-37.0	68	1.414
20131203	6630.311	jguarroflo	406/5000	-1.11	-17.8	177	1.255
20131203	6630.318	bmauclaire	300/16000	-1.64	-37.4	30	1.257
20131204	6631.284	jguarroflo	406/5000	-1.36	-42.4	81	1.276
20131205	6632.287	jguarroflo	406/5000	-1.12	-56.2	178	1.503
20131206	6633.274	jguarroflo	406/5000	-1.16	-41.3	162	1.385
20131207	6634.345	bmauclaire	300/16000	-1.43	-41.0	80	1.299
20131209	6636.237	jguarroflo	406/5000	-0.94	-64.5	221	1.395
20131215	6642.293	jguarroflo	406/5000	-0.76	-63.3	270	1.067
20131218	6644.525	kgraham	305/13500	-1.06	-45.3	171	1.131
20131223	6650.248	jguarroflo	406/5000	-0.28	-161.7	565	1.079
20140101	6658.605	csawicki	356/15000	-0.12	-69.6	854	0.721
20140107	6665.266	jguarroflo	406/5000	0.27	-90.3	643	0.521
20140108	6666.261	jguarroflo	406/5000	0.04	-69.2	1479	0.710
20140729	6868.478	vdesnoux	200/12000	-4.02	-16.7	234	1.076
20140805	6875.509	epollmann	400/20000	-3.59	-26.7	246	1.389

Date (YYYYMMDD)	HJD $-2\,450\,000$	Observer	tel size/R (mm)/	EW (Å)	RV (km s^{-1})	width (km s^{-1})	V/R
20140806	6876.470	bmauclaire	300/16000	-4.09	-8.2	232	1.174
20140823	6893.470	epollmann	400/20000	-4.33	-8.3	230	1.092
20140828	6897.605	bmauclaire	300/16000	-4.30	-4.2	229	1.006
20140913	6914.346	epollmann	400/20000	-4.46	-17.8	233	1.000
20140916	6917.375	pfosanelli	280/17000	-4.84	-14.5	228	0.874
20140918	6919.400	pfosanelli	280/17000	-4.71	-11.5	225	0.875
20140923	6924.339	epollmann	400/20000	-5.13	-15.6	224	0.892
20140923	6924.423	pfosanelli	280/17000	-5.19	-15.0	230	0.931
20140926	6927.332	pberardi	235/13500	-5.34	-11.1	231	0.876
20140926	6927.418	pfosanelli	280/17000	-5.09	-12.1	229	0.859
20140927	6928.373	jguarroflo	406/5000	-5.40	-10.2	235	0.864
20140927	6928.375	plailly	203/15000	-5.35	0.3	223	0.876
20140930	6931.308	pberardi	235/13500	-5.30	-11.4	229	0.869
20141001	6932.344	jguarroflo	406/5000	-5.30	-10.0	232	0.863
20141002	6933.332	jguarroflo	406/5000	-5.42	-12.9	233	0.872
20141003	6934.303	epollmann	400/20000	-4.98	-13.6	224	0.868
20141003	6934.333	jguarroflo	406/5000	-5.33	-13.2	232	0.886
20141003	6934.338	fhoupert	280/15000	-6.07	-10.0	236	0.878
20141005	6936.333	pberardi	235/13500	-5.60	-14.2	230	0.902
20141008	6939.364	jguarroflo	406/5000	-5.66	-10.9	232	0.915
20141011	6942.456	pfosanelli	280/17000	-5.48	-10.6	227	0.922
20141013	6944.373	jguarroflo	406/5000	-5.67	-14.9	230	0.945
20141014	6945.305	pfosanelli	280/17000	-5.43	-11.8	224	0.967
20141016	6947.316	mpujol	300/11000	-4.82	-10.6	210	0.952
20141016	6947.358	jguarroflo	406/5000	-5.67	-11.3	231	1.029
20141017	6948.357	jguarroflo	406/5000	-5.64	-16.9	227	1.052
20141017	6948.393	mleonardi	235/7800	-5.37	-19.9	222	1.005
20141017	6948.421	plailly	203/15000	-5.89	-13.6	225	1.047
20141018	6949.356	epollmann	400/20000	-5.49	-14.0	222	1.061
20141018	6949.407	fhoupert	280/15000	-6.69	-9.9	233	1.040
20141019	6950.398	pfosanelli	280/17000	-5.67	-11.1	224	1.054
20141019	6950.409	mleonardi	235/7800	-5.54	-13.7	217	1.104
20141020	6951.274	pberardi	235/13500	-5.64	-14.5	224	1.095
20141020	6951.359	jguarroflo	406/5000	-5.84	-12.3	231	1.066
20141021	6952.341	jguarroflo	406/5000	-6.12	-13.8	231	1.042
20141022	6953.321	jguarroflo	406/5000	-5.86	-6.0	229	1.078
20141022	6953.359	mleonardi	235/7800	-5.82	-15.2	223	1.093
20141023	6954.299	mpujol	300/11000	-5.38	-12.2	218	1.118
20141023	6954.389	mleonardi	235/7800	-5.74	-14.2	221	1.087
20141024	6955.387	mleonardi	235/7800	-5.42	-15.0	221	1.093
20141026	6956.673	csawicki	356/15000	-6.35	-15.9	230	1.100
20141026	6957.349	mleonardi	235/7800	-6.19	-10.0	232	1.107
20141026	6957.386	pfosanelli	280/17000	-5.79	-11.1	225	1.078
20141028	6959.329	mleonardi	235/7800	-6.03	-12.4	227	1.194
20141029	6960.308	mpujol	300/11000	-5.33	-8.0	217	1.151
20141029	6960.350	nmont+mmann	250/17000	-5.24	-12.2	228	1.153
20141030	6961.270	mpujol	300/11000	-5.52	-8.9	220	1.134
20141030	6961.317	nmont+mmann	250/17000	-5.66	-20.2	225	1.176
20141030	6961.336	mleonardi	235/7800	-6.04	-10.7	225	1.118
20141031	6961.649	csawicki	356/15000	-6.22	-16.3	230	1.154
20141101	6963.397	mleonardi	235/7800	-6.19	-10.0	229	1.208
20141101	6963.427	fhoupert	280/15000	-6.69	-9.8	235	1.139
20141105	6967.388	jguarroflo	406/5000	-6.19	-10.9	231	1.102
20141106	6968.332	jguarroflo	406/5000	-5.97	-13.3	230	1.093

Date (YYYYMMDD)	*HJD* −2 450 000	Observer	tel size/*R* (mm)/	*EW* (Å)	*RV* (km s^{-1})	width (km s^{-1})	*V/R*
20141106	6968.386	mleonardi	235/7800	-6.15	-10.8	231	1.042
20141108	6970.324	jguarroflo	406/5000	-5.96	-10.7	229	1.030
20141112	6974.323	jguarroflo	406/5000	-5.95	-15.1	228	1.062
20141113	6975.245	epollmann	400/20000	-5.94	-14.4	220	1.087
20141113	6975.303	mleonardi	235/7800	-6.33	-10.9	229	1.063
20141114	6976.315	pberardi	235/13500	-5.98	-13.4	226	1.057
20141115	6976.641	csawicki	356/15000	-6.59	-8.8	231	1.029
20141115	6977.390	jguarroflo	406/5000	-5.91	-9.0	228	1.057
20141116	6978.369	jguarroflo	406/5000	-6.19	-7.7	230	1.023
20141119	6981.335	mleonardi	235/7800	-6.72	-12.6	230	1.033
20141120	6982.252	pberardi	235/13500	-5.97	-16.7	223	1.052
20141121	6982.596	kgraham	305/13500	-5.60	-1.7	217	1.000
20141121	6982.691	csawicki	356/15000	-6.08	-14.4	223	1.040
20141121	6983.223	epollmann	400/20000	-6.57	-13.4	232	1.085
20141126	6988.328	jguarroflo	406/5000	-6.24	-13.5	227	0.976
20141127	6988.592	csawicki	356/15000	-6.82	-11.5	229	1.004
20141127	6989.359	epollmann	400/20000	-10.11	-11.4	222	0.972
20141202	6994.307	jguarroflo	406/5000	-6.60	-15.0	230	0.913
20141205	6997.325	jguarroflo	406/5000	-6.54	-13.0	227	0.946
20141206	6998.345	jguarroflo	406/5000	-6.85	-20.5	229	0.931
20141207	6999.218	pberardi	235/13500	-6.40	-18.4	223	0.962
20141213	7004.622	csawicki	356/15000	-6.53	-21.7	222	0.934
20141218	7010.291	mleonardi	235/7800	-6.88	-18.5	226	0.861
20141220	7011.639	csawicki	356/15000	-6.90	-13.0	225	0.943
20141229	7020.622	csawicki	356/15000	-7.13	-11.1	224	0.945
20150101	7024.267	mleonardi	235/7800	-7.30	-9.5	225	0.911
20150103	7026.311	mleonardi	235/7800	-7.44	-19.5	230	0.921
20150105	7028.312	mleonardi	235/7800	-7.41	-11.2	223	0.957
20150111	7034.296	mleonardi	235/7800	-7.70	-13.2	226	1.044
20150605	7178.584	ogarde	400/11000	-10.02	-10.1	222	0.959
20150628	7201.574	jmontier	355/17000	-11.05	-8.9	222	1.047
20150711	7214.578	epollmann	400/20000	-10.98	-4.6	222	1.042
20150716	7219.740	tlester	310/8000	-11.22	-2.9	224	1.037
20150721	7224.569	othizy	280/10000	-10.41	-13.5	216	1.067
20150723	7227.487	jterry	300/9000	-10.29	-8.2	211	1.074
20150725	7229.453	ogarde	400/11000	-10.92	-6.5	217	1.029
20150802	7236.520	jmontier	355/17000	-11.64	-7.1	221	0.992
20150805	7240.463	epollmann	400/20000	-10.87	-12.8	218	0.971
20150809	7243.737	tlester	310/8000	-11.84	-11.2	220	0.978
20150813	7247.539	afavaro	200/17000	-12.04	-10.5	219	0.980
20150817	7252.425	bmauclaire	300/16000	-12.11	-12.4	215	0.931
20150819	7254.462	jterry	300/9000	-11.41	-21.2	213	0.957
20150819	7254.488	adebruin	280/5800	-12.69	-12.8	221	0.967
20150821	7256.488	afavaro	200/17000	-12.37	-13.9	218	0.959
20150825	7260.380	ogarde	400/11000	-13.06	-14.5	218	0.973
20150826	7261.394	jterry	300/9000	-11.23	-16.3	211	0.972
20150828	7262.737	tlester	310/8000	-13.13	-14.5	222	0.934
20150902	7268.416	adebruin	280/5800	-13.16	-11.1	221	0.945
20150907	7273.412	ogarde	400/11000	-13.48	-8.2	219	0.945
20150917	7282.710	tlester	310/8000	-13.53	-9.4	218	0.973
20150927	7293.370	epollmann	400/20000	-14.40	-7.4	221	1.063
20150928	7294.297	adebruin	280/5800	-14.29	-8.7	222	1.038
20150930	7296.354	adebruin	280/5800	-13.53	-1.3	217	1.032
20151002	7298.362	epollmann	400/20000	-14.21	-6.1	219	1.062

Date (YYYYMMDD)	HJD $-2\,450\,000$	Observer	tel size/R (mm)/	EW (Å)	RV (km s^{-1})	width (km s^{-1})	V/R
20151008	7303.627	tlester	310/8000	-14.61	-6.3	220	1.048
20151012	7308.347	adebruin	280/5800	-14.04	-2.9	217	1.013
20151022	7318.415	jguarroflo	406/5000	-14.60	-6.6	218	0.990
20151023	7319.404	jguarroflo	406/5000	-14.56	-7.9	219	0.987
20151026	7322.296	adebruin	280/5800	-15.31	-8.8	221	0.974
20151026	7322.401	epollmann	400/20000	-15.25	-9.0	220	1.000
20151029	7325.305	adebruin	280/5800	-15.28	-8.2	220	0.964
20151030	7326.495	tlester	310/8000	-14.90	-9.7	218	0.988
20151031	7327.267	ogarde	400/11000	-15.31	-8.9	217	0.984
20151031	7327.349	fhoupert	280/15000	-16.30	-9.6	220	0.984
20151101	7328.310	vdesnoux	235/15000	-14.32	-12.3	215	1.000
20151102	7329.222	adebruin	280/5800	-15.28	-13.1	220	0.979
20151102	7329.296	epollmann	400/20000	-14.90	-10.6	218	1.004
20151104	7330.585	kgraham	305/13500	-14.33	-10.1	214	0.984
20151104	7330.704	csawicki	510/17000	-13.10	-12.5	206	0.981
20151106	7333.245	ogarde	400/11000	-15.16	-11.6	217	0.982
20151107	7333.650	csawicki	510/17000	-13.44	-7.7	208	0.965
20151108	7335.244	pberardi	235/13500	-14.77	-14.6	216	0.961
20151108	7335.278	ckreider	430/600	-13.72	-15.9	248	-
20151108	7335.422	fhoupert	280/15000	-16.00	-12.7	217	0.952
20151109	7336.310	afavaro	200/17000	-15.92	-13.2	218	0.958
20151109	7336.320	jguarroflo	406/5000	-14.90	-13.1	218	0.942
20151110	7337.347	jguarroflo	406/5000	-15.00	-16.8	218	0.968
20151111	7338.335	jguarroflo	406/5000	-14.83	-15.1	218	0.954
20151113	7340.395	jguarroflo	406/5000	-15.02	-15.7	217	0.938
20151115	7342.329	plailly	203/15000	-15.05	-13.1	213	0.949
20151118	7345.267	pberardi	235/13500	-15.06	-12.3	216	0.939
20151118	7345.274	afavaro	200/17000	-15.63	-14.1	217	0.945
20151123	7350.396	jguarroflo	406/5000	-14.77	-17.7	217	0.948
20151125	7352.334	jguarroflo	406/5000	-14.79	-12.4	218	0.955
20151127	7354.351	jguarroflo	406/5000	-14.99	-15.5	217	0.954
20151129	7356.217	pberardi	235/13500	-15.01	-14.4	215	0.949
20151211	7367.673	csawicki	510/17000	-13.36	-4.1	207	0.955
20151217	7374.283	pfosanelli	280/16000	-14.21	-5.3	209	1.008
20151221	7378.271	jguarroflo	406/5000	-14.84	-5.4	215	1.027
20151222	7379.327	jguarroflo	406/5000	-15.23	-6.1	217	1.032
20151229	7386.227	mleonardi	235/7800	-15.75	-3.4	216	1.061
20151230	7387.265	jguarroflo	406/5000	-15.67	-3.7	217	1.025
20160121	7409.247	jguarroflo	406/5000	-14.58	-71.0	224	1.199
20160123	7411.243	jguarroflo	406/5000	-14.62	-57.9	221	1.078
20160125	7413.236	ogarde	400/11000	-15.10	-11.1	213	0.970
20160205	7424.237	ogarde	400/11000	-14.55	-13.6	209	0.978
20160710	7579.583	othizy	280/11000	-15.66	-11.1	211	1.015
20160717	7586.584	afavaro	200/17000	-15.73	-13.3	210	0.968
20160725	7594.526	afavaro	200/17000	-15.25	-14.1	209	1.041
20160728	7597.533	othizy	280/11000	-16.05	-17.4	211	1.019
20160812	7613.455	jterry	280/17000	-14.73	-13.7	206	0.941
20160817	7618.464	ogarde	400/11000	-16.28	-9.5	210	0.982
20160819	7619.686	tlester	310/8000	-16.50	-8.1	213	0.973
20160823	7624.487	tlemoult	356/11000	-16.18	-8.9	210	0.988
20160824	7625.431	adebruin	280/5800	-17.44	-9.7	215	1.005
20160825	7626.463	adebruin	280/5800	-17.36	-5.9	215	1.004
20160826	7626.548	jterry	280/17000	-16.67	-7.3	212	1.006
20160829	7630.426	adebruin	280/5800	-17.79	-6.5	215	1.011

Date (YYYYMMDD)	*HJD* −2 450 000	Observer	tel size/*R* (mm)/	*EW* (Å)	*RV* (km s⁻¹)	width (km s⁻¹)	*V/R*
20160830	7631.431	fhoupert	280/15000	-18.07	-3.3	213	1.015
20160905	7637.393	adebruin	280/5800	-17.68	-8.7	215	1.010
20160906	7638.397	adebruin	280/5800	-17.21	-4.6	215	1.032
20160906	7638.401	jterry	280/17000	-16.73	-6.7	211	1.066
20160907	7639.402	adebruin	280/5800	-17.57	-10.3	215	1.018
20160909	7641.476	fhoupert	280/15000	-18.06	-1.9	213	1.029
20160912	7644.356	adebruin	280/5800	-17.57	-0.2	216	1.012
20160913	7645.387	adebruin	280/5800	-17.74	-2.0	217	1.040
20160914	7646.402	adebruin	280/5800	-17.62	-4.5	215	1.034
20160924	7656.404	afavaro	200/17000	-17.94	-7.6	212	0.980
20160924	7656.464	epollmann	400/20000	-17.40	-8.2	213	1.008
20160925	7657.356	ebertrand	203/18000	-18.00	-5.9	212	0.956
20160928	7660.398	fhoupert	280/15000	-18.86	-8.4	214	0.976
20161002	7664.344	adebruin	280/5800	-17.90	-4.0	212	0.987
20161004	7666.388	ogarde	400/11000	-17.87	-11.6	210	0.966
20161004	7666.496	epollmann	400/20000	-17.92	-11.6	213	0.974
20161006	7668.313	adebruin	280/5800	-18.04	-7.8	215	0.964
20161010	7671.564	tlester	310/8000	-17.97	-11.9	212	0.960
20161017	7679.289	adebruin	280/5800	-18.39	-15.7	216	0.988
20161020	7681.667	csawicki	510/17000	-17.12	-15.2	207	0.994
20161028	7690.353	ebertrand	203/13000	-18.66	-13.1	213	0.970
20161030	7691.636	csawicki	510/17000	-17.42	-14.5	208	0.965
20161030	7692.335	fhoupert	280/15000	-19.17	-11.9	213	0.958
20161031	7693.224	ogarde	400/11000	-18.16	-12.4	211	0.939
20161031	7693.269	adebruin	280/5800	-18.51	-10.8	216	0.975
20161107	7699.661	kgraham	305/13500	-18.02	-9.6	209	0.943
20161108	7700.510	tlester	310/8000	-18.19	-10.1	212	0.964
20161115	7708.362	ogarde	400/11000	-18.42	-5.5	211	0.966
20161124	7716.576	csawicki	510/17000	-17.01	-2.9	206	1.020
20161124	7717.210	adebruin	280/5800	-19.24	-6.9	216	1.008
20161126	7719.195	ogarde	400/11000	-18.59	-3.1	211	1.035
20161127	7720.268	epollmann	400/20000	-16.14	-10.8	204	1.045
20161128	7721.206	adebruin	280/5800	-19.28	1.2	217	1.023
20161129	7722.204	adebruin	280/5800	-19.23	1.3	216	1.023
20161204	7727.238	ogarde	400/11000	-18.60	-3.3	212	1.035
20161213	7736.266	ogarde	400/11000	-17.94	-5.1	211	0.993
20170726	7963.526	ctq+mm	127/12000	-20.73	-11.8	212	1.015
20170731	7965.538	vdesnoux	200/15000	-20.52	-9.8	211	1.045
20170805	7971.392	ctq+mm	127/12000	-19.93	-6.6	208	1.038
20170806	7972.468	ogarde	400/11000	-20.69	0.7	209	1.071
20170814	7980.379	ctq+mm	127/12000	-20.19	-5.5	211	1.022
20170817	7983.484	othizy	280/11000	-20.17	-4.4	209	1.053
20170826	7992.360	othizy	280/11000	-20.38	-6.5	210	0.984
20170828	7994.474	adebruin	200/5800	-24.45	-1.1	210	0.985
20170908	8005.378	ogarde	400/11000	-20.00	-15.9	208	0.975
20170909	8006.350	ctq+mm	127/12000	-19.97	-11.8	211	0.996
20170919	8016.373	adebruin	200/5800	-22.39	-25.1	218	1.013
20170921	8017.708	tlester	310/13000	-19.51	-15.6	208	1.002
20170921	8018.371	adebruin	200/5800	-20.31	-19.8	211	0.987
20170921	8018.379	othizy	280/11000	-20.23	-16.8	209	1.026
20170928	8025.326	othizy	280/11000	-20.08	-14.8	209	1.006
20170929	8026.324	ogarde	400/11000	-19.79	-8.9	208	0.996
20171001	8028.290	ctq+mm	127/12000	-19.85	-15.7	210	1.012
20171006	8033.280	ctq+mm	127/12000	-19.97	-13.6	210	0.986

Date (YYYYMMDD)	HJD $-2\,450\,000$	Observer	tel size/R (mm)/	EW (Å)	RV (km s^{-1})	width (km s^{-1})	V/R
20171006	8033.298	othizy	280/11000	-20.37	-13.1	209	1.011
20171009	8036.394	jguarroflo	406/9000	-19.94	-11.1	210	0.960
20171010	8037.264	othizy	280/11000	-20.25	-10.0	209	0.956
20171010	8037.372	jguarroflo	406/9000	-19.95	-11.1	209	0.972
20171011	8038.375	jguarroflo	406/9000	-20.26	-11.9	210	0.966
20171011	8038.396	fhoupert	280/15000	-22.04	-8.3	212	0.968
20171012	8039.373	jguarroflo	406/9000	-20.32	-10.8	210	0.976
20171012	8039.374	jterry	280/17000	-21.55	-1.9	211	0.956
20171013	8040.318	ogarde	400/11000	-20.57	-6.7	209	0.971
20171014	8041.392	jguarroflo	406/9000	-20.12	-8.7	210	0.990
20171017	8044.357	jguarroflo	406/9000	-19.73	-7.7	209	0.989
20171020	8047.253	othizy	280/11000	-20.15	-6.8	208	1.032
20171020	8047.400	jguarroflo	406/9000	-20.03	-6.7	208	0.993
20171020	8047.431	ebertrand	203/13000	-20.66	-1.8	210	1.007
20171022	8049.394	jguarroflo	406/9000	-19.90	-6.5	209	0.989
20171025	8052.324	jguarroflo	406/9000	-20.19	-4.1	208	0.980
20171026	8052.618	kgraham	305/13500	-21.46	-3.4	211	1.027
20171027	8054.402	jguarroflo	406/9000	-20.09	-4.4	208	0.982
20171029	8056.243	ctq+mm	127/12000	-20.54	-8.1	209	1.020
20171029	8056.338	jguarroflo	406/9000	-20.21	-4.2	208	1.002
20171030	8057.321	fhoupert	280/15000	-21.96	-3.7	210	1.052
20171031	8058.305	ogarde	400/11000	-21.42	-3.7	210	1.056
20171031	8058.370	jguarroflo	406/9000	-20.49	-4.1	209	1.060
20171101	8059.252	othizy	280/11000	-20.84	-5.8	208	1.076
20171101	8059.391	jguarroflo	406/9000	-20.07	-4.1	208	1.028
20171103	8061.347	jguarroflo	406/9000	-20.34	-3.2	208	1.035
20171109	8067.326	jguarroflo	406/9000	-20.43	-12.0	209	1.042
20171111	8069.250	ctq+mm	127/12000	-20.81	-3.9	210	1.040
20171113	8071.399	jguarroflo	406/9000	-19.86	-10.7	207	1.023
20171114	8072.277	othizy	280/11000	-21.14	-7.9	211	1.042
20171115	8073.245	othizy	280/11000	-20.95	-8.0	210	1.048
20171116	8074.358	jguarroflo	406/9000	-20.31	-10.7	209	1.016
20171121	8079.347	jguarroflo	406/9000	-19.95	-14.0	207	0.978
20171122	8080.212	ogarde	400/11000	-21.55	-9.6	212	0.991
20171123	8081.214	othizy	280/11000	-20.57	-9.9	209	0.998
20171124	8081.575	csawicki	510/17000	-18.97	-10.1	204	0.991
20171125	8083.373	jguarroflo	406/9000	-20.28	-11.5	207	0.989
20171128	8086.365	jguarroflo	406/9000	-20.02	-11.5	208	0.993
20171130	8088.380	jguarroflo	406/9000	-20.41	-12.0	208	1.005
20171204	8092.209	othizy	280/11000	-21.01	-17.0	209	1.004
20171204	8092.350	jguarroflo	406/9000	-19.88	-18.6	207	1.016
20171212	8100.214	ogarde	400/11000	-21.40	-13.7	211	1.032
20171216	8104.224	ctq+mm	127/12000	-20.64	-21.1	210	1.018
20171218	8106.351	jguarroflo	406/9000	-20.12	-14.2	208	1.011
20180108	8126.580	csawicki	510/17000	-20.82	-8.3	208	0.964
20180114	8133.225	fhoupert	280/15000	-22.46	-3.9	211	1.009
20180616	8285.587	othizy	280/11000	-21.61	-10.8	212	0.973
20180716	8315.539	othizy	280/11000	-21.84	-7.2	213	1.172
20180721	8321.459	ebryssinck	280/9500	-22.04	-0.3	213	1.166
20180727	8327.444	ctq+mm	127/12000	-22.73	-6.7	216	1.105
20180810	8341.485	ogarde	400/11000	-21.85	-11.8	209	1.061
20180812	8342.532	fhoupert	280/15000	-23.72	-15.3	212	1.053
20180818	8348.539	fhoupert	280/15000	-24.06	-16.9	211	1.075
20180822	8352.516	trodda	235/600	-21.47	9.6	245	-

| Date (YYYYMMDD)	HJD $-2\,450\,000$	Observer	tel size/R (mm)/	EW (Å)	RV (km s^{-1})	width (km s^{-1})	V/R
20180822	8353.393	ctq+mm	127/12000	-24.04	-12.5	214	1.058
20180825	8356.512	fhoupert	280/15000	-24.32	-16.0	211	1.094
20180826	8357.395	ogarde	400/11000	-21.92	-17.1	206	1.152
20180908	8369.533	fhoupert	280/15000	-25.28	-11.8	211	1.071
20180910	8372.393	adebruin	200/5800	-23.45	-10.0	210	1.023
20180910	8372.468	afavaro	200/17000	-16.93	-6.4	205	1.036
20180913	8375.304	adebruin	200/5800	-23.32	-15.7	209	1.034
20180915	8377.391	fhoupert	280/15000	-24.98	-8.3	209	1.047
20180917	8379.353	ctq+mm	127/12000	-24.55	-1.3	212	1.073
20180917	8379.407	fhoupert	280/15000	-24.81	-7.6	208	1.049
20180917	8379.427	othizy	280/11000	-23.50	-8.9	207	1.058
20180919	8381.416	othizy	280/11000	-23.45	-9.8	207	1.061
20180920	8382.365	othizy	280/11000	-23.60	-8.8	207	1.079
20180920	8382.441	jguarroflo	406/9000	-23.23	-5.5	207	1.055
20180928	8390.474	jguarroflo	406/9000	-23.40	-6.7	206	1.065
20180929	8391.395	fhoupert	280/15000	-25.28	-4.7	209	1.053
20180929	8391.414	ogarde	400/11000	-25.33	-3.1	212	1.048
20181003	8395.333	othizy	280/11000	-24.12	-6.5	207	1.091
20181003	8395.379	jguarroflo	406/9000	-22.79	-4.5	204	1.061
20181004	8396.354	othizy	280/11000	-23.97	-6.4	206	1.063
20181008	8400.338	adebruin	200/5100	-24.16	-7.2	207	1.078
20181008	8400.365	fhoupert	280/15000	-25.81	-4.1	207	1.072
20181009	8401.273	adebruin	200/5100	-24.24	-5.9	208	1.053
20181009	8401.327	othizy	280/11000	-24.17	-6.5	205	1.064
20181010	8402.307	adebruin	200/5100	-24.11	-2.7	208	1.108
20181011	8403.255	adebruin	200/5100	-23.82	-7.1	207	1.076
20181018	8410.304	adebruin	200/17000	-23.83	-16.1	208	1.031
20181018	8410.369	fhoupert	280/15000	-25.15	-5.0	207	1.063
20181023	8415.322	fhoupert	280/15000	-25.31	-6.8	209	1.007
20181023	8415.407	jguarroflo	406/9000	-23.51	-8.7	207	1.025
20181024	8416.298	othizy	280/11000	-23.88	-9.1	207	1.009
20181025	8416.540	kgraham	305/12000	-20.82	-7.5	198	1.017
20181102	8425.413	jguarroflo	406/9000	-23.31	-12.3	205	0.963
20181103	8426.295	fhoupert	280/15000	-25.54	-11.0	209	0.970
20181108	8430.961	tbohlsen	280/14000	-25.04	-8.3	208	0.945
20181110	8433.332	ebryssinck	280/15000	-25.14	-12.3	205	0.921
20181112	8434.986	tbohlsen	280/14000	-24.39	-12.8	208	0.950
20181114	8437.242	adebruin	280/17000	-22.20	-14.6	204	0.923
20181114	8437.260	othizy	280/11000	-23.84	-15.1	206	0.962
20181115	8438.277	ebryssinck	280/15000	-24.23	-13.5	207	0.934
20181116	8439.246	othizy	280/11000	-23.45	-15.3	205	0.944
20181116	8439.273	ctq+mm	127/12000	-25.31	-10.3	211	0.929
20181116	8439.304	fhoupert	280/15000	-25.26	-12.5	208	0.915
20181118	8441.222	othizy	280/11000	-23.75	-15.7	207	0.943
20181119	8441.602	jdaglen	356/13000	-24.83	-14.7	209	0.937
20181119	8441.954	tbohlsen	280/14000	-24.26	-13.8	208	0.956
20181126	8448.994	tbohlsen	280/14000	-24.09	-7.6	210	0.954
20181126	8449.348	jguarroflo	406/9000	-23.16	-11.9	207	0.954
20181128	8450.699	astiewing	280/17000	-23.86	-10.5	209	0.952
20181209	8461.609	astiewing	280/17000	-24.14	-5.0	209	0.905
20181210	8463.337	jguarroflo	406/9000	-23.22	-6.0	208	0.909
20181216	8469.244	jguarroflo	406/9000	-23.32	-3.2	208	0.927
20181226	8479.264	ogarde	400/11000	-24.53	0.0	211	0.936
20190103	8487.214	ogarde	400/11000	-24.27	-0.9	213	0.970
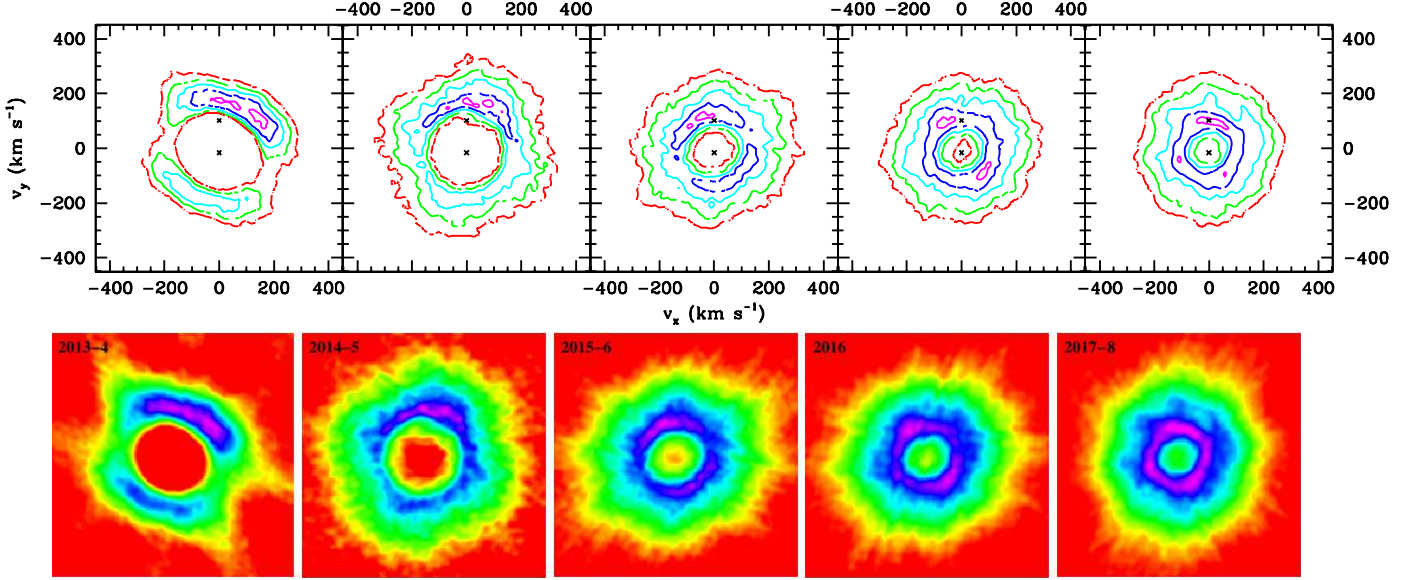
Figure 4: Doppler maps for Hα in the five observing seasons 2013-4, 2014-5, 2015-6, 2016, 2017-8. In the contour plots, the magenta, blue, cyan, green, and red contours correspond to amplitudes of 95%, 80%, 65%, 50%, and 35% of the maximum emission. The two crosses indicate the velocities of the secondary (top) and primary (bottom) according to the semi-amplitudes K derived by Bjorkman et al. (2002). The bottom color images provide the same maps as images. These maps correspond to a slice at $v_z = -10 \, \mathrm{km \, s^{-1}}$, the mean RV value of the system (see Fig. 1) - calculations made with values of +10 or $0 \, \mathrm{km \, s^{-1}}$ provide similar results, however.

Date (YYYYMMDD)	HJD $-2\,450\,000$	Observer	tel size/R (mm)/	EW (Å)	RV (km s^{-1})	width (km s^{-1})	V/R
20190106	8490.274	jguarroflo	406/9000	-23.21	-2.9	211	0.985
20190115	8499.274	jguarroflo	406/9000	-22.83	-6.2	211	0.948
20190121	8505.215	fhoupert	280/15000	-25.33	-7.8	215	0.906
20190121	8505.265	jguarroflo	406/9000	-22.67	-7.5	211	0.915

Table 1: Continued.